Causal effect of the tropical Pacific sea surface temperature on the Upper Colorado River Basin spring precipitation

Siyu Zhao[1] · Jiaying Zhang[2]

Abstract

The Colorado River is one of the most important rivers in the southwestern U.S., with ∼90% of the total flow originating from the Upper Colorado River Basin (UCRB). The UCRB April–July streamflow is well-correlated to the UCRB spring precipitation. It is known that the UCRB precipitation is linked to an El Niño-like sea surface temperature (SST) pattern, but the causal effect of the tropical Pacific SST on the UCRB spring precipitation is still uncertain. Here, we apply a Granger causality approach to understand the causal effect of the tropical Pacific averaged SST in previous three seasons (winter, fall, and summer) on the UCRB averaged precipitation in spring in observations and two climate models. In observations, only the winter SST has Granger causal effect (with p-value ∼0.05) on spring precipitation, while historical simulations of the two climate models overestimate the causal effect for winter and fall (with p-value < 0.01 and < 0.05, respectively) due to model biases. Moreover, future projections of the two climate models show divergent causal effects, especially for the scenario with high anthropogenic emissions. The divergent projections indicate that (1) there are large uncertainties in model projections of the causal effect of the tropical Pacific SST on UCRB spring precipitation and (2) it is uncertain whether climate models can reliably capture changes in such causality. These uncertainties may result in large uncertainties in seasonal forecasts of the UCRB hydroclimate under global climate change.

Keywords Upper Colorado River Basin precipitation · Seasonal predictability · Sea surface temperature · Granger causality · Climate change · Global climate model

1 Introduction

The Colorado River is one of the most important rivers in the southwestern U.S. It provides water for nearly 40 million people, irrigates ∼20,000 km^2 of land, and generates more than 4,200 megawatts of hydroelectric power per year (U.S. Bureau of Reclamation 2012). The Upper Colorado River Basin (UCRB), defined as the catchment area upstream of the U.S. Geological Survey stream gauge at Lees Ferry, Arizona, provides ∼90% of the streamflow for the Colorado River (Jacobs 2011). The streamflow during April–July has large contribution to the annual total flow and mountain snowpacks accumulated from previous fall to spring provide major sources for the streamflow (e.g., Aziz et al. 2010; Bracken et al. 2010; Werner and Yeager 2013; Xiao et al. 2018).

Recently, a significant negative trend of April–July streamflow was observed over the UCRB (e.g., Xiao et al. 2018). The negative trend could be attributed to sustained drought conditions (Reynolds et al. 2015; Woodhouse et al. 2016; Xiao et al. 2018; Hoerling et al. 2019; Hobbins and Barsugli 2020; Milly and Dunne 2020). Warm-season temperature also has negative effects on the UCRB streamflow and such effects will become more evident and problematic as warming continues (McCabe et al. 2017). The climate change impacts on the UCRB streamflow have been widely investigated (e.g., Barnett et al. 2005; Alley et al. 2007; Harding et al. 2012; Ficklin et al. 2013; Vano et al. 2014; Vano and Lettenmaier 2014; Ayers et al. 2016; Udall and Overpeck 2017; Solander et al. 2018). For example, Solander et al. (2018) found that more severe changes in streamflow for Colorado River Basin (CRB; including both

✉ Siyu Zhao
  siyu_zhao@atmos.ucla.edu

[1] Department of Atmospheric and Oceanic Sciences, University of California, Los Angeles, Los Angeles, CA, USA

[2] School of Civil and Environmental Engineering, Georgia Institute of Technology, Atlanta, GA, USA

upper and lower basins) watersheds with high elevations will probably occur in a warmer climate in the future. Under global warming, regions where water supply is dominated by melting snowpacks tend to have decreasing snowfall and increasing rainfall in winter and early melting time of winter snowpacks (Barnett et al. 2005). Such changes will potentially lead to a shift in the peak of streamflow from spring to early spring or winter and likely influence future water availability.

Given that regional precipitation, snowpack, among other climate data (such as temperature) have direct impact on the streamflow, those variables have been used for short-lead (lead time shorter than four months) operational hydrologic and water supply seasonal forecasts for the Colorado River (e.g., Franz et al. 2003; Pagano et al. 2009; Werner 2011; Najafi et al. 2012; Werner and Yeager 2013; Fleming and Goodbody 2019). For example, the Colorado Basin River Forecast Center (CBRFC) produces both seasonal flood and seasonal water supply forecasts. Especially, the CBRFC provides monthly updates of seasonal forecasts of the UCRB streamflow starting in January using an ensemble streamflow prediction approach (e.g., Werner and Yeager 2013). The U.S. Department of Agriculture's Natural Resources Conservation Service provides seasonal water supply forecasts in the western U.S. adopting a probabilistic nonlinear regression technique, which includes supervised and unsupervised machine learning, nonparametric statistical modeling, ensemble modeling, and evolutionary optimization (Fleming and Goodbody 2019). For long-lead (lead time longer than four months) seasonal forecasts of the UCRB streamflow, Pacific sea surface temperatures (SSTs) have been widely used (e.g., Regonda et al. 2006; Switanek et al. 2009; Bracken et al. 2010; Lamb et al. 2011; Oubeidillah et al. 2011; Sagarika et al. 2015, 2016). Recently, Zhao et al. (2021) derived Pacific SST Predictors (PSP) from a dipole pattern over the Pacific (30° S–65° N) that is correlated with the lagging UCRB streamflow. The long-lead prediction skills shown in their study are probably associated with the emergence of strong PSP–streamflow correlations in recent decades.

The role of the Pacific SST (predictor for long-lead streamflow prediction) in modulating the CRB precipitation (predictor for short-lead streamflow prediction) has been evaluated (e.g., Hidalgo and Dracup 2003; Kim et al. 2006). The SST variability associated with the El Niño–Southern Oscillation (ENSO; Cai et al. 2015a) provides dominant interannual variability in the equatorial Pacific. A warm phase of the ENSO leads to increasing precipitation in summer over the upper basin, while the cold phase of the ENSO leads to decreasing precipitation in winter over the lower basin (Wang and Ting 2000; Kim et al. 2006). For the UCRB, warm season precipitation was found to be more

strongly linked to the El Niño (Niño 3 index) than cold season precipitation did (Hidalgo and Dracup 2003).

Global climate models (GCMs) were applied to understand the trend, variability, and other properties of the UCRB precipitation. For example, Gautam and Mascaro (2018) evaluated nineteen models from Fifth Phase of the Coupled Model Intercomparison Project (CMIP5) and found that these models tend to overestimate the climatological mean of the annual precipitation over the CRB up to 140% and slightly underestimate the interannual variability of the annual precipitation. Ayers et al. (2016) compared projected hydrologic conditions over the UCRB between CMIP3 and CMIP5 models. They found that 57% of the UCRB region shows a significantly increasing trend in precipitation throughout the twenty-first century in CMIP5 models, but only 5% in CMIP3 models. By applying U.S. Bureau of Reclamation's climate projection datasets, Udall and Overpeck (2017) argued that an increase in precipitation will probably moderate the decline of the Colorado River streamflow due to a temperature increase, while there is no model agreement on future projections of precipitation changes.

In addition, GCMs have been widely used to study characteristics and potential changes of the Pacific SST variability (e.g., Deser et al. 2012; Sheffield et al. 2013; Cai et al. 2015a, b, 2018; Newman et al. 2016). Cai et al. (2014, 2015b) found that both El Niño and La Niña events may increase under greenhouse warming in both CMIP3 and CMIP5 models. Their results showed that high frequency of El Niño events is probably due to projected warmer eastern equatorial Pacific than the surrounding ocean waters and high occurrence of atmospheric convection in the east basin. On the contrary, high frequency of La Niña events is likely due to projected faster warming of the Maritime continent (i.e., lands between Indian and Pacific Oceans, including countries of Indonesia, Philippines and Papua New Guinea, etc.) than the central Pacific and increased upper ocean vertical temperature gradients. However, there is no agreement on future projections of ENSO variability (e.g., Stevenson 2012; Power et al. 2013; Kim et al. 2014; Chen et al. 2017).

Despite of aforementioned studies, the linkage between the Pacific SST and UCRB precipitation remains unclear, especially the linkage under different climate scenarios. A Granger causality approach has been applied to study the causality between two fields. For example, Wang et al. (2004) and Mosedale et al. (2006) applied Granger causality approach to understand the causal effect of preceding SST anomalies on the wintertime North Atlantic Oscillation (Wang et al. 2004; Mosedale et al. 2006). McGraw and Barnes (2018) applied Granger causality to ENSO and land surface temperature and suggested that Granger causality approach is superior to traditional lagged regression/correlation approach when one or more datasets have large memory.

Previous studies have not paid adequate attention on the UCRB spring precipitation. Its influence on the UCRB streamflow during April–July is somewhat overlooked due to the great impact of mountain snowpacks on streamflow. In fact, the correlation coefficient between the spring precipitation averaged over the UCRB and total natural flow during April–July at Lees Ferry (the downstream gauge of the UCRB) is 0.60 from 1950 to 2014 (significant at the 0.001 level according to Student's *t* test) (see the text and Fig. S1 in the Supplementary Material). This result indicates that in addition to mountain snowpacks, the UCRB spring precipitation is also well-correlated to the UCRB streamflow during the runoff season. Therefore, the goal of this study is to investigate the causal effect of the previous-season Pacific SST on the UCRB spring [March–May (MAM)] precipitation in observations and in historical and Shared Socioeconomic Pathway (SSP; Meinshausen et al. 2020) simulations of two CMIP6 models using the Granger causality approach.

2 Data and methodology

2.1 Observational datasets

The monthly averaged precipitation is from National Oceanic and Atmospheric Administration (NOAA) Climate Prediction Center (CPC) Unified Gauge-Based Analysis with a resolution of 0.25° from 1949 to 2014 (Chen et al. 2008). The data after 2014 are not included in order to be consistent with CMIP6 models' historical simulations. The monthly averaged SST is from the Hadley Centre Sea Ice and Sea Surface Temperature (HadISST) with a resolution of 1.0° from 1949 to 2014 (Rayner et al. 2003). The monthly mean zonal and meridional winds and geopotential height come from National Centers for Environmental Prediction–National Center for Atmospheric Research (NCEP–NCAR) reanalysis with a resolution of 2.5° and 17 pressure levels in the vertical ranging from 1000 to 10 hPa from 1949 to 2014 (Kalnay et al. 1996). The daily mean zonal and meridional winds and specific humidity are also from NCEP–NCAR reanalysis. We choose the NCEP–NCAR data because it has long temporal coverage. The monthly total natural flow data for the stream gauge at Lees Ferry is obtained from Bureau of Reclamation (Prairie and Callejo 2005).

2.2 CMIP6 model simulations

Following Zhao et al. (2017), two state-of-the-art models of CMIP6 archives—the NCAR Community Earth System Model version 2 (CESM2; Danabasoglu et al. 2020) and the NOAA Geophysical Fluid Dynamics Laboratory Earth System Model version 4 (GFDL-ESM4; Dunne et al. 2020)—are analyzed in this study. The two models are widely used in

the U.S. for climate assessment and have relatively high resolutions (around 1-degree spatial resolution and a minimum of 3-hourly temporal output). Historical simulations (for the period of 1949–2014) from the two models are analyzed and then compared with parallel observational analyses. The external forcings of historical simulations include well-mixed greenhouse gases, anthropogenic sulfate aerosol, volcanic aerosol, ozone, land-use change, organic carbon, black carbon, etc. Pre-industrial control (piControl) simulations with non-evolving pre-industrial conditions are used to compare with historical simulations and to detect the influence of external forcings versus model biases. Since the length of piControl simulations is 500 years, we divide the 500-year simulations into seven members (a total of 462 years are used). Each member has length of 66 years, consistent with the length of historical simulations (1949–2014; total of 66 years).

Three main SSP simulations (for the period of 2035–2100) from the two models are also used, including the SSP245, SSP370, and SSP585 scenarios (Meinshausen et al. 2020). The SSP245 represents a "middle of the road" scenario, with the radiative forcing level of 4.5 W m^{-2} by 2100. The SSP370 is a medium–high scenario within the "regional rivalry" socio-economic family. The SSP585 indicates a high reference scenario within the "fossil-fueled development" family. Since available ensemble member is very limited for piControl and SSP simulations, here we only include one ensemble for each simulation. The details of these simulations are summarized in Table 1.

2.3 Granger causality

Granger causality approach is applied to determine the causal effect of the tropical Pacific SST on the UCRB precipitation. Granger (1969) defined causality as follows: if the history of an independent variable X has causal effect on the future state of a dependent variable Y and such causal effect is stronger than that using the history of Y itself, then X has Granger causal effect on Y. We establish the direction of the Granger causal pathway, i.e., from SST to precipitation. We examine three lead seasons: winter [December–February (DJF)], fall [September–November (SON)], and summer [June–August (JJA)], separately. For each lead season, we calculate the time series of the UCRB averaged spring precipitation, the time series of UCRB averaged precipitation in the lead season, and the time series of domain averaged SST anomaly over the tropical Pacific (15° S–15° N/90° W–170° W) in the lead season. Since the Granger causality approach requires processes to be linear and stationary (e.g., Mosedale et al. 2006; McGraw and Barnes 2018), we assume that the relationship between the Pacific SST and spring precipitation is linear and remove the linear trend of the above time series.

Table 1 The details of the CESM2 and GFDL-ESM4 models

Model abbr.	Simulations	Ensemble number	Period	Atmosphere grids (lon×lat)	Ocean grids (lon×lat)
CESM2	Historical	1	1949–2014	288×192	384×320
	SSP245		2035–2100		
	SSP370		2035–2100		
	SSP585		2035–2100		
	piControl		1–462 years		
GFDL-ESM4	Historical	1	1949–2014	288×180	720×576
	SSP245		2035–2100		
	SSP370		2035–2100		
	SSP585		2035–2100		
	piControl		1–462 years		

Following Wang et al. (2004) and Mosedale et al. (2006), we derive the relationship between SST and precipitation using a vector autoregressive model with exogenous variables, which can be expressed as:

$$Precip_t = \alpha_1 + \beta_1 Precip_{t-\tau} + \gamma_1 SST_{t-\tau} + \varepsilon_1, \tag{1}$$

where $\alpha_{()}, \beta_{()}$, and $\gamma_{()}$ are regression coefficients, $\varepsilon_{()}$ is the error term (also called residual), and τ is the lead time. In Eq. 1, to predict precipitation at time t, only one lead time (i.e., $t - \tau$) is applied for the past precipitation and SST. Such setting is different from that in previous studies (e.g., Wang et al. 2004; Mosedale et al. 2006) that apply lead times from $t - 1$ to $t - \tau$ (where $\tau \geq 1$). In our study, we will determine the causality for each lead time separately. Then, we estimate the restricted form of Eq. 1 where the causal variable ($SST_{t-\tau}$) is eliminated, which is done statistically by restricting γ_1 to zero:

$$Precip_t = \alpha_2 + \beta_2 Precip_{t-\tau} + \varepsilon_2. \tag{2}$$

Next, we apply both F-test and Chi-squared (χ^2) test to examine whether the restricted estimates (i.e., Eq. 2) are significantly different from the unrestricted estimates (i.e., Eq. 1). The F-test and Chi-squared test are statistical hypothesis tests in which the test statistic has an F-distribution and Chi-squared distribution, respectively, under the null hypothesis. We calculate the F statistic as follows:

$$S = \frac{(RSS_r - RSS_u)/m}{RSS_u/(NY - n)}. \tag{3}$$

In Eq. 3, $RSS_{()}$ is the sum of residual (ε) squares; the subscripts r and u refer to the restricted (Eq. 2) and unrestricted (Eq. 1) forms, respectively; NY is the number of observations (the number of total years); m is the number of coefficients that are restricted to zero (i.e., γ_1) and $m = 1$ here; and n is the number of coefficients in the unrestricted form of the equation and $n = 3$. The Chi-squared statistic is as follows:

$$S = NY\left(\log \frac{|\Omega_r|}{|\Omega_u|} \right), \tag{4}$$

where $|\Omega_{()}|$ is the determinant of the covariance matrix of the residuals. Since the residuals are a vector here, $|\Omega_{()}|$ is also equal to $RSS_{()}$. Finally, the test statistics are evaluated against the F and Chi-squared distribution, respectively, and p-value is computed. The null hypothesis is that the independent variable eliminated from Eq. 1 (i.e., the past value of SST) does not have causal effect on the dependent variable (i.e., spring precipitation). To reject the null hypothesis of no causality between the two variables at 95% confidence interval, the p-value of the statistic should be less than 0.05. We also detect the causality in the opposite direction, i.e., from precipitation to SST. To do so, the "$Precip$" and "SST" in Eqs. 1 and 2 are substituted with "SST" and "$Precip$", respectively. Finally, caveats to the Granger causality approach are discussed in Sect. 4.

3 Results

3.1 UCRB spring precipitation and preceding Pacific SST

Figure 1a shows the climatological mean of the spring precipitation over the UCRB in the observation. Precipitation with large values (> 1.5 mm day^{-1}) occurs over mountainous regions. Lower latitudes generally have low precipitation (< 0.5 mm day^{-1}). Figure 1b, c shows that large variability and positive trend of the precipitation occur over mountainous regions. For the two climate models (CESM2 and GFDL-ESM4), historical simulations are compared with the observation for the same period (1950–2014) but with lower spatial resolutions (Fig. 1d–i). The two models well capture the spatial pattern of the climatological mean spring
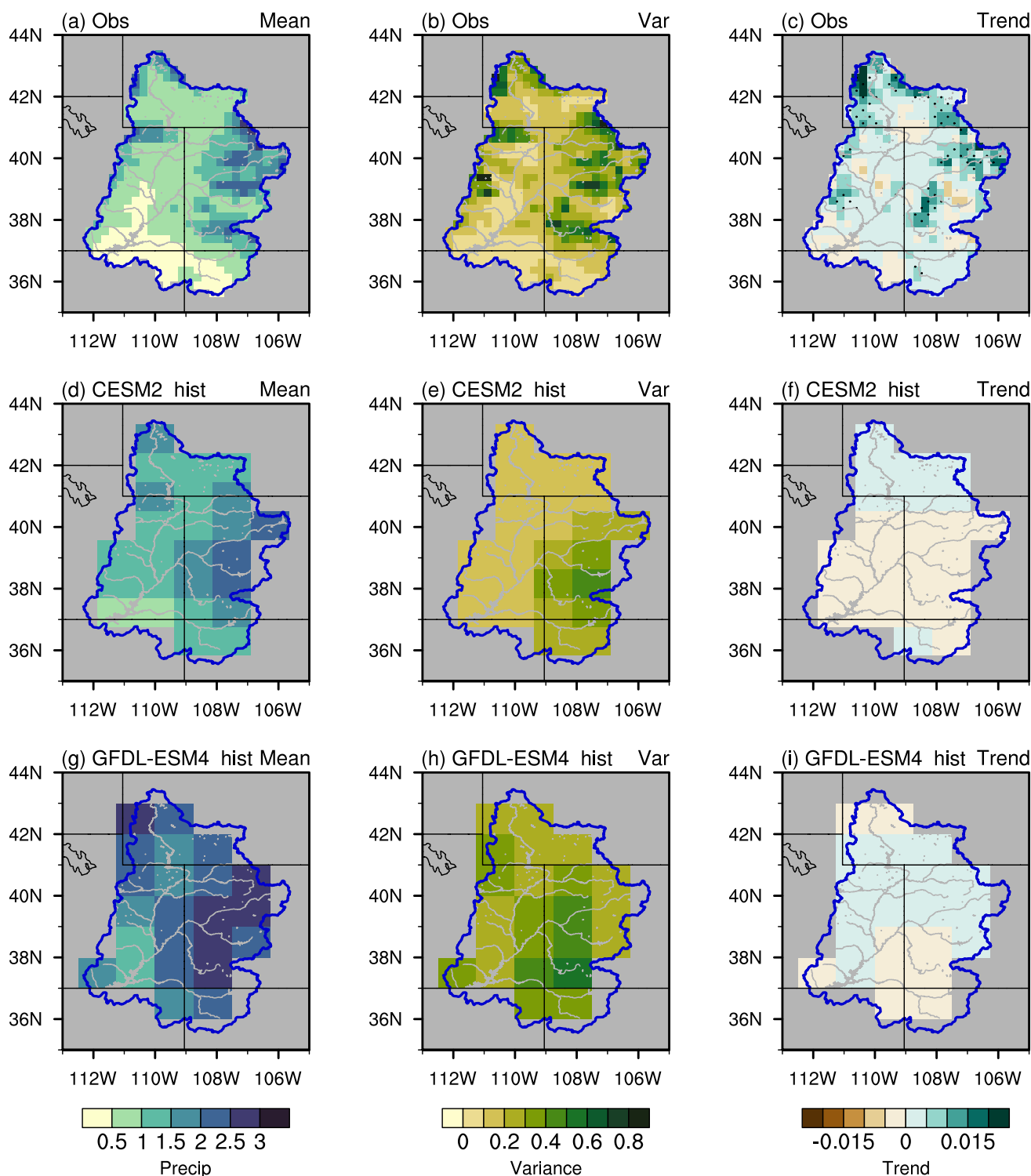
Fig. 1 **a–c** Climatological mean (mm day^{-1}), variance ((mm day^{-1})^2), and trend (regression coefficient; mm day^{-1} per year) of precipitation during spring over the UCRB in the observation. **d–i** Same as **a–c**, but for historical simulations of two models. Dots denote regression coefficients significant at 0.05 level (according to Student's *t* test)

precipitation, but overestimate the magnitude, especially for the GFDL-ESM4. In addition, there are some discrepancies between the climate models and observations for the

precipitation variance. For example, the CESM is unable to capture the large variance over the western boundary of the UCRB, while the GFDL-ESM4 overestimates the variance

over lower latitudes (e.g., around 37°–38° N). The two models fail to capture the trend shown in the observation for the period of 1950–2014.

Figure 2a shows the climatological mean of monthly mean domain averaged precipitation in both observation and historical simulations of the two climate models. It is noted that the spring precipitation in the observation is slightly higher than that of the annual mean, while modeled spring precipitation is much higher than modeled annual mean precipitation. This result further indicates an overestimation of the UCRB spring precipitation in the

two climate models. Figure 2b shows the empirical probability distribution function (PDF) of the UCRB domain-mean spring precipitation for years between 1950 and 2014 in both observation and two models. The most frequent value of the spring precipitation (1.0 mm day^{-1} in observation) is overestimated by the two models (1.3 and 2.3 mm day^{-1} in the CESM2 and GFDL-ESM4, respectively). Previous studies have documented the bias of the model-simulated precipitation (e.g., Zhao et al. 2016, 2017; Gautam and Mascaro 2018). We correct the bias by calculating the ratio of the climatological mean spring

Fig. 2 **a** Climatological mean of monthly mean (solid lines) and annual mean (dashed lines) precipitation (mm day^{-1}) averaged over the UCRB in both observation and historical simulations of the two models. **b** PDF (%) of the UCRB domain-mean spring precipitation for 1950–2014 in observation and historical simulations of the two models. **c** Same as **b**, but for bias-corrected modeled precipitation
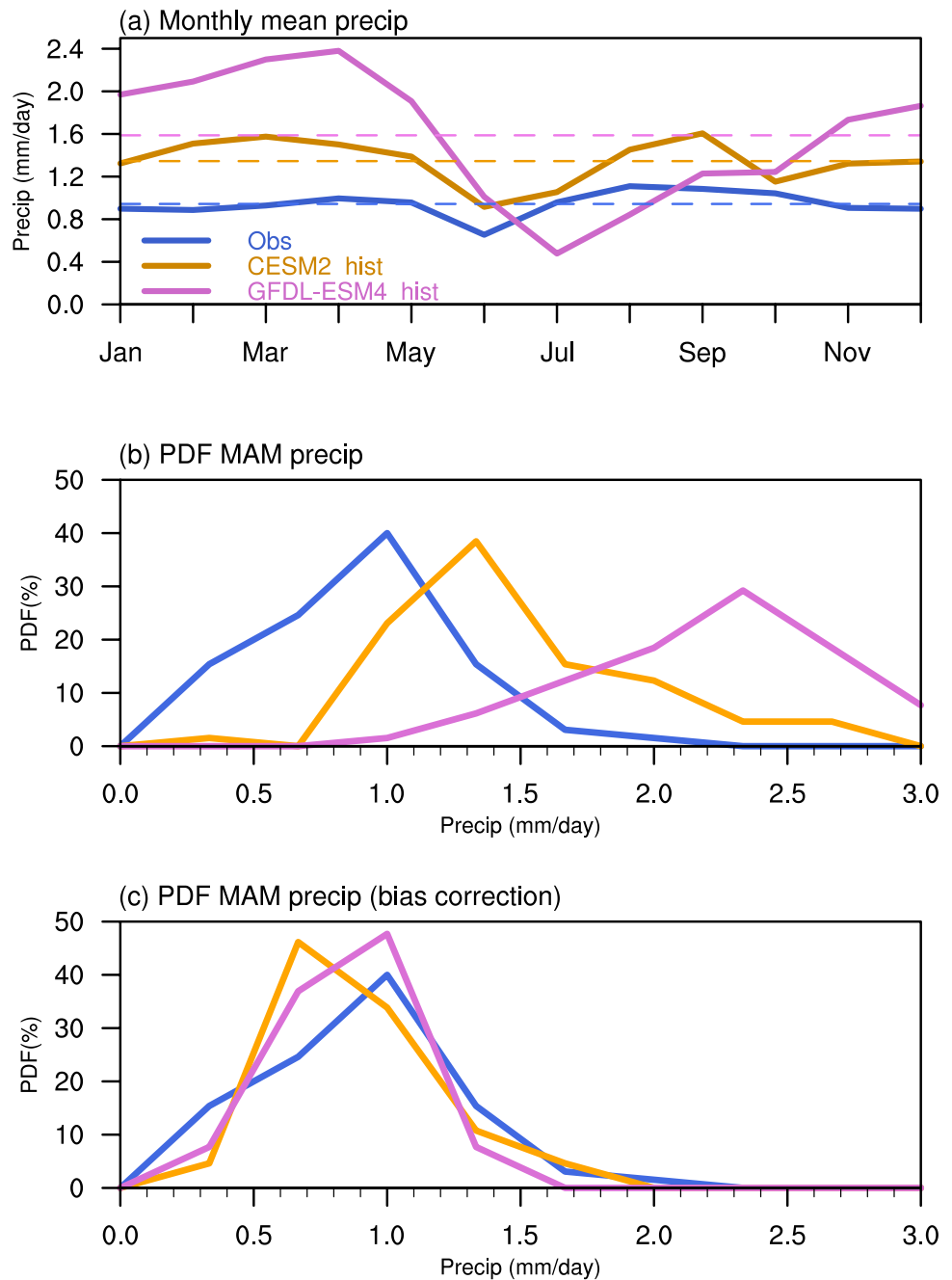
precipitation between climate model and observation (i.e., Fig. 1a–c) and then applying the ratio to modeled spring precipitation in each year (Zhao et al. 2016, 2017). The resultant modeled precipitation shares similar values and PDF with those in the observation (Fig. 2c). We notice that such bias-correction approach has very small impact on the results of correlation/causality in following sections.

We calculate the variance of previous winter, fall, and summer Pacific SST in both observation and two climate models. In general, large-variance region shifts from the eastern Pacific to central Pacific from summer to winter, and such characteristics are well captured by the two models, especially the CESM2 (Fig. 3). However, the two models overestimate the SST variance, especially during winter. In addition, discrepancies of the SST trend are shown between the climate models and observation (Fig. S2). The misrepresentation of the trend is probably due to the insufficiency of climate models to represent the real physical world. Nevertheless, we do not need to worry about the trend because it is completely removed in the following analyses.

3.2 Causal effect of SST on precipitation with historical data

In this section, we assess the casual effect of the Pacific SST on the UCRB spring precipitation in both observation and historical simulations of the two climate models. We compute correlation coefficients between the detrended UCRB domain-mean spring precipitation and detrended Pacific SST in the previous winter, fall, and summer, separately. Figure 4a shows the SST–precipitation correlation map, which reveals that an El Niño-like SST pattern during winter is significantly (at the 0.05 level according to Student's t test) linked to the following UCRB spring precipitation in the observation. Note that the correlation between spring precipitation and spring SST is similar to that between spring precipitation and winter SST (Fig. S3 vs Fig. 4a), indicating that the lagged correlation signal in previous winter persists into spring. The correlation drops rapidly when the lead time extends to the previous summer (Fig. 4b, c). Both models' historical simulations can capture the El Niño-like correlation pattern and the weaker correlation with longer
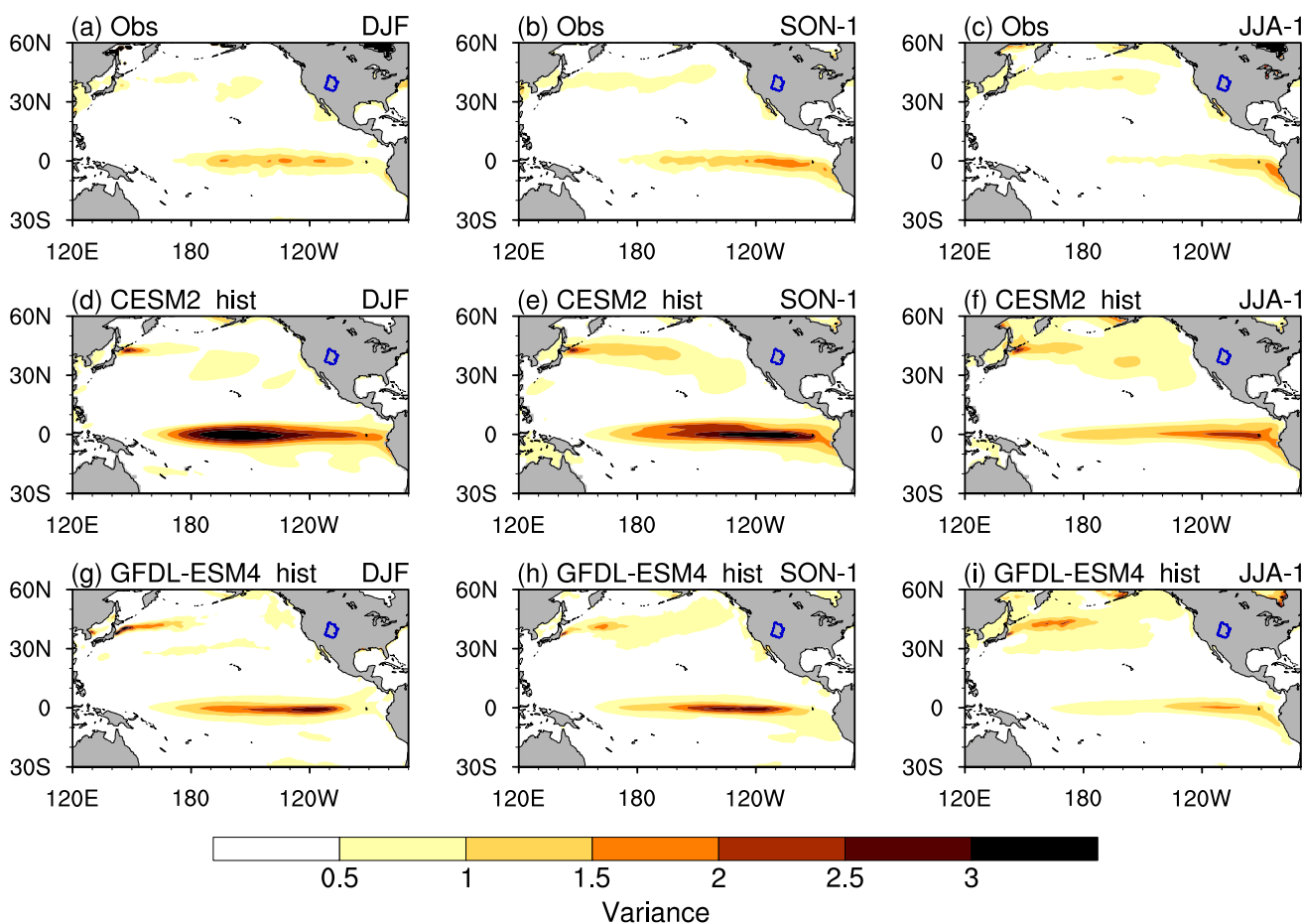
Fig. 3 **a–c** Variance ($(°C)^2$) of previous winter, fall, and summer SST in observation. **d–i** Same as **a–c**, but for historical simulations of the two models
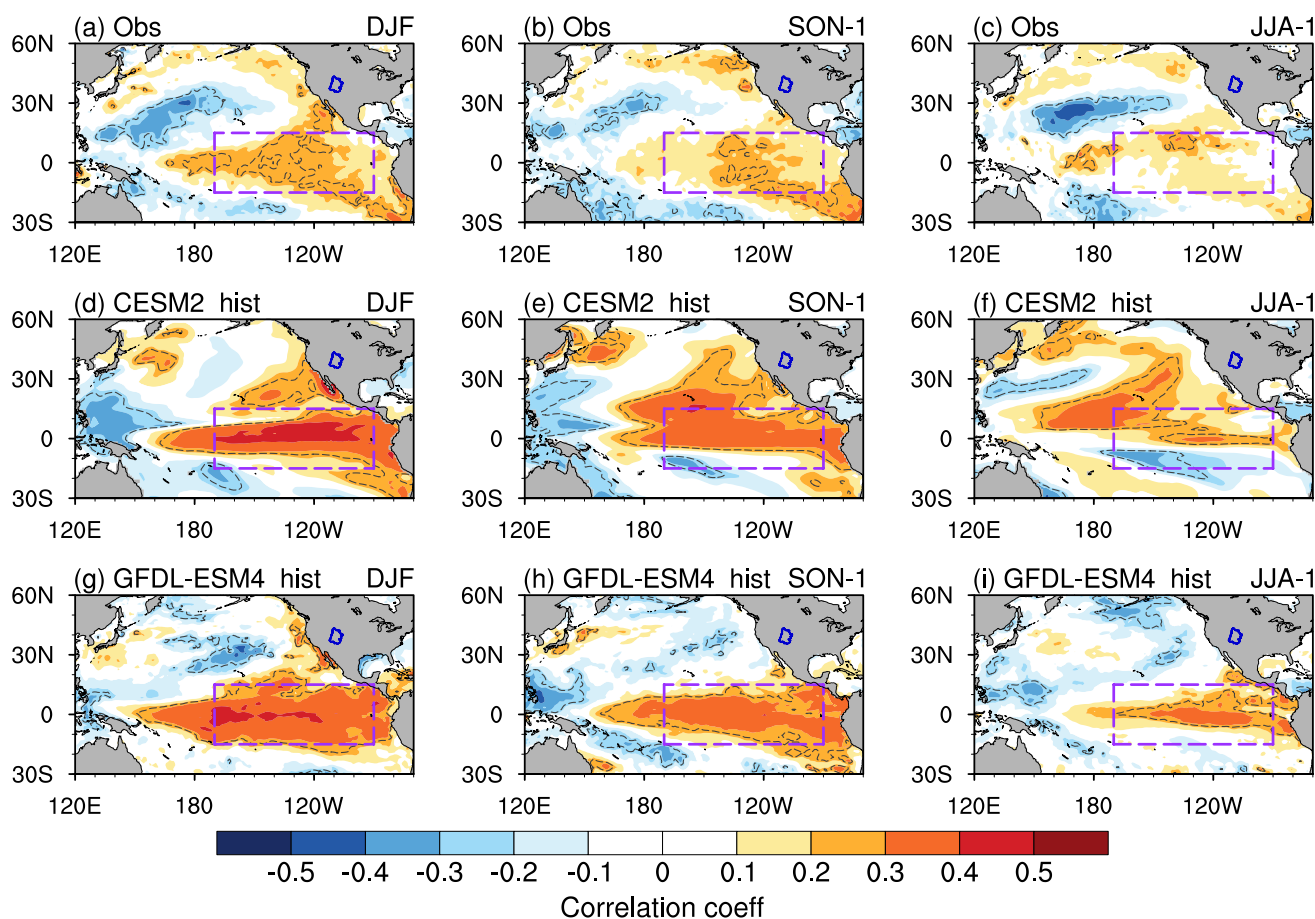
Fig. 4 a–c Correlation coefficients (shading) between the UCRB domain-mean spring precipitation and the previous winter, fall, and summer SST from observation. **b, c** Same as **a** but for previous fall and summer SST, respectively. **d–i** Same as **a–c**, but for historical simulations of the two models. Contours denote correlation coeffi-

cients significant at 0.05 level (according to Student's *t* test). The purple box shows the domain selected for calculating the tropical Pacific averaged SST. The blue curve over North America shows the domain of the UCRB

lead times (Fig. 2d–i). However, modeled correlation coefficients are overestimated for winter and fall, especially over the equatorial Pacific, and the spatial pattern of the coefficients is either spatially shifted (GFDL-ESM4) or distorted (CESM2) for summer.

To understand whether the difference between historical simulations and observation is from external forcings or model biases, we calculate correlation coefficients between the two fields for each member (each has the data of 65 years) of the piControl simulations. Figure 5 shows the averaged correlation coefficients among the seven members of each model. In general, the correlation patterns agree with those of historical simulations, but with an even larger overestimation of the correlation. Such result suggests that piControl simulations have larger biases than historical simulations and external forcings in historical simulations reduce the model biases.

Next, we apply the Granger causality approach to determine the causal effect of three lead-season (winter, fall, and

summer) tropical Pacific SST on spring precipitation (see Sect. 2.3 for the methodology). For each lead season, the three detrended time series applied are: the UCRB averaged spring precipitation, UCRB averaged precipitation in the lead season, and high-correlation domain averaged SST anomaly over the tropical Pacific (within the purple box in Fig. 4) in the lead season. Figure 6a shows the scatter plot of the correlation coefficient (between the time series of winter SST and that of spring precipitation) versus *p*-value of the *F*-test of the Granger causality. For the observation, the *p*-value of Granger causality is significant at 0.05 level, indicating that the winter SST has causal effect on UCRB spring precipitation. For historical simulations of the two models, the *p*-value (< 0.01) is smaller than that of the observation (Fig. 6a), consistent with the overestimation of the correlation between the two fields in the climate models (Fig. 4d, g). For the lead time of previous fall, the *p*-value of the *F*-test in the observation is greater than 0.1, which is not as significant as those in the two models (*p*-values < 0.05)
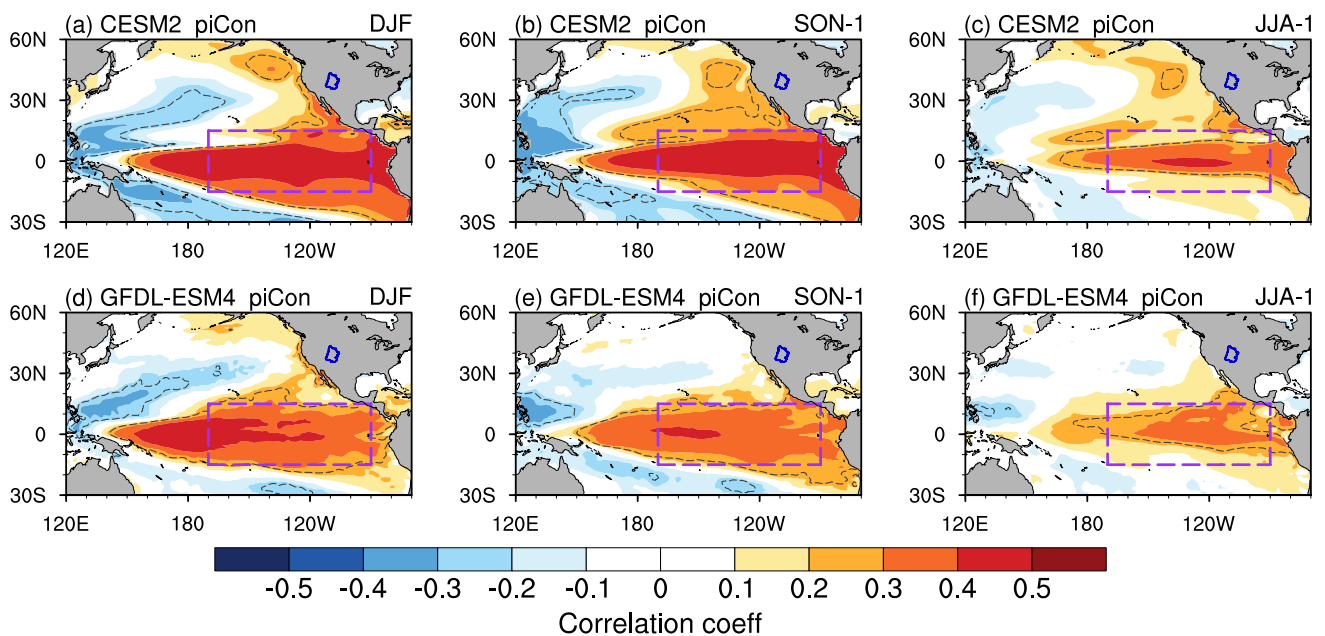
Fig. 5 a–f Same as Fig. 4, but for the averaged correlation coefficients of seven members of piControl simulations of the two models

(Fig. 6b), indicating that the causal effect of SST on precipitation is insignificant in the observation but significant in the two models. For the previous summer, the *p*-values of the observation and two models are greater than 0.1, indicating no causality at 90% confidence level (Fig. 6c). The *p*-values of the Chi-squared test are slightly smaller than those of the *F*-test (Fig. 6d–f). Therefore, the tropical Pacific SST has causal effect on UCRB spring precipitation with lead time of one season in the observation and up to two seasons in the two models.

The causal effect (measured by the *p*-value) in piControl simulations is even stronger than that in historical simulations, especially for summer (Fig. 7). Such result further suggests that piControl simulations have larger biases than the historical simulation and external forcings in historical simulations reduce these biases. In addition, we show the causality in the opposite direction, i.e., from previous-season precipitation to spring SST. As expected, no causality could be detected in observation and historical simulations of the two models (Fig. S4). It is interesting to note that even though the correlation between fall precipitation and spring SST is significant at the 0.05 level, the *p*-value of the Granger causality is insignificant (Fig. S4b, e). This result confirms the finding in a previous study that lagged correlation is likely to overestimate the relationship when the variable has large memory (McGraw and Barnes 2018).

To find out the circulation pattern linked to the casual effect of SST on precipitation, we calculate correlation coefficients between the UCRB spring precipitation and previous-season streamfunction (computed by monthly zonal

and meridional winds) at 500 hPa. Note that here we do not expect to find any causality among the three variables (precipitation, SST, and streamfunction). In the observation, the correlation pattern during winter exhibits a dipole structure over the North Pacific, with strong negative correlation over the mid-latitude North Pacific and positive correlation over the tropical North Pacific (Fig. 8a). In addition, the correlation between winter streamfunction and tropical Pacific averaged (the purple box in Fig. 4) winter SST shows a similar spatial pattern albeit with larger magnitudes (Fig. S5). This result suggests that the tropical Pacific winter SST and UCRB spring precipitation can be linked by a dipole circulation pattern over the North Pacific. This dipole pattern disappears in fall and summer and changes to a negative correlation pattern over the North Pacific (Fig. 8b, c), associated with no causal effect of SST during fall and summer on spring precipitation (Fig. 6). The modeled precipitation–streamfunction correlation in winter are similar to the observation, but with stronger magnitudes (Fig. 8d, g), accompanied by overestimations of the causal effect (Fig. 6) and the variance of streamfunction (Fig. S6) during winter. Large discrepancies in the spatial pattern of the precipitation–streamfunction correlation could also be seen with longer lead times (Fig. 8e, f, h, i).

3.3 Future projections of the causality

In this section, we investigate the change of the causality under different climate scenarios. The long-term (2036–2100) domain averaged UCRB spring precipitation
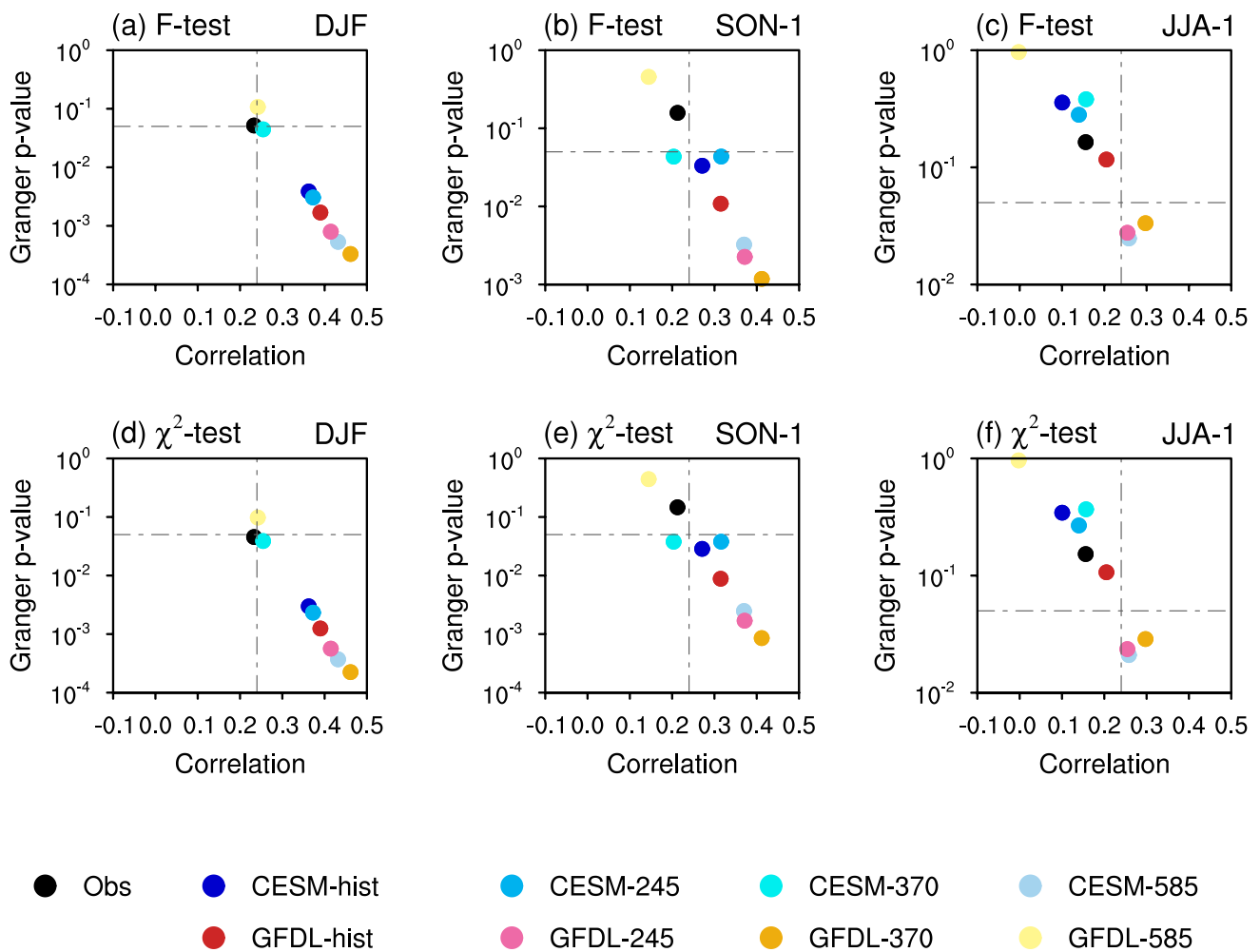
Fig. 6 a–c Scatter plot for correlation coefficient versus *p*-value of the *F*-test from the Granger causality in the observation and historical and SSP simulations of the two models. The correlation is for tropical Pacific domain-mean winter, fall, and summer SST and UCRB domain-mean spring precipitation. The direction of the Granger causality is from SST to precipitation. **d–f** Same as **a–c**, but for the Chi-squared test of the Granger causality. The dashed lines denote the thresholds significant at 0.05 level

in SSP scenarios is generally similar to that in historical simulations for both models (Fig. 9a). When anthropogenic emissions increase (from SSP245 to SSP585), the variance of the UCRB spring precipitation increases for CESM2 but decreases for GFDL-ESM4 (Fig. 9b), consistent with the finding that models do not have agreement on the change of precipitation projections (Udall and Overpeck 2017). For previous-season SST, the variance increases as anthropogenic emissions increase in the two models (Fig. 10). The westward shift of the peak variance from summer to winter is more apparent in CESM2 than GFDL-ESM4.

Figure 11 shows correlation coefficients between the detrended UCRB averaged spring precipitation and detrended previous-season Pacific SST in future projections. Since the trend of SST (Fig. S7) has been removed, the SST warming due to anthropogenic emissions will not influence the relationship between SST and precipitation.

The two climate models exhibit divergent projections of the SST–precipitation correlation. For example, the correlation in SSP585 scenario is the strongest among the three scenarios in the CESM2 model, but the weakest in the GFDL-ESM4 model. When the lead time is longer, both models show a weaker correlation, consistent with the results in observation and historical simulations. The Granger causality agree with the correlation result, that is, a very large difference between the two models' SSP585 scenario (Fig. 6). The *p*-value of the Granger causality for the CESM2 (GFDL-ESM4) in the SSP585 scenario is < 0.001 (> 0.05) for winter, < 0.01 (> 0.1) for fall, and < 0.05 (~ 1.0) for summer. Such divergent projections indicate that (1) there are large uncertainties in model projections of the causal effect of the tropical Pacific SST on UCRB precipitation and (2) it is uncertain whether GCMs can reliably capture changes in such causality.
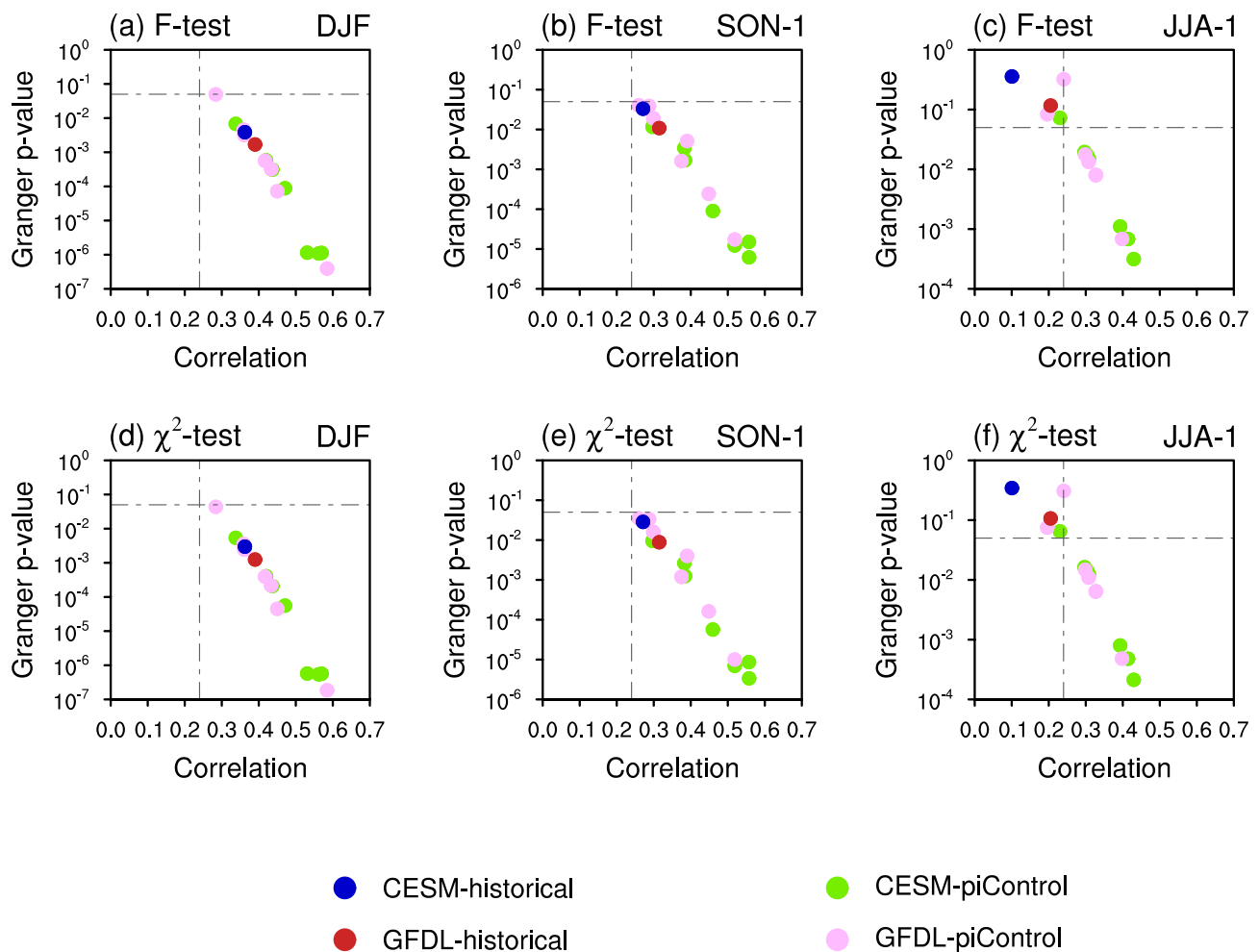
Fig. 7 Same as Fig. 6, but for historical simulations and seven members of piControl simulations of the two models

The divergent causal effects in the SSP585 scenario could be due to the different nature of the projected UCRB spring precipitation and tropical Pacific SST. As shown in Figs. 9 and 10, some basic characteristics (e.g., variance and mean) of the precipitation and SST are different between CESM and GFDL-ESM4 and such differences may lead to different causal effects. Another reason may arise from model representations of atmospheric circulation anomaly. Figure 12 shows correlation coefficients between the detrended UCRB spring precipitation and previous-season streamfunction at 500 hPa under three SSP scenarios in the two models. Similar to historical simulations, the dipole circulation pattern over the North Pacific is pronounced in winter for all three scenarios, corresponding to the El Niño-like SST pattern. Consistent with the results of the causal analysis, the precipitation–streamfunction correlation in the SSP585 scenario is the largest in magnitude among the three scenarios for the CESM2 model but the smallest for the GFDL-ESM4 model. This result indicates that the difference in the causal effect may also result from the different representations of

the dipole circulation pattern in the SSP585 scenario. We also notice that if the dipole circulation pattern is captured by the model, the resultant causal effect of SST on precipitation can also be captured. This suggests that the model's skill in representing such causality is positively correlated with its capability in representing the dipole circulation pattern.

4 Discussion

In this study, we assume the relationship between the Pacific SST and spring precipitation is linear and thus apply the linear vector autoregressive model with exogenous variables. As suggested by previous studies (e.g., Wu et al. 2005; Hsieh et al. 2006; Fleming and Dahlke 2014), the relationship between precipitation/streamflow and ENSO can be nonlinear (e.g., quadratic or parabolic) over some regions of North America (e.g., U.S. and southern Canada). Such nonlinear relationship is worth exploration in the future (see Attanasio
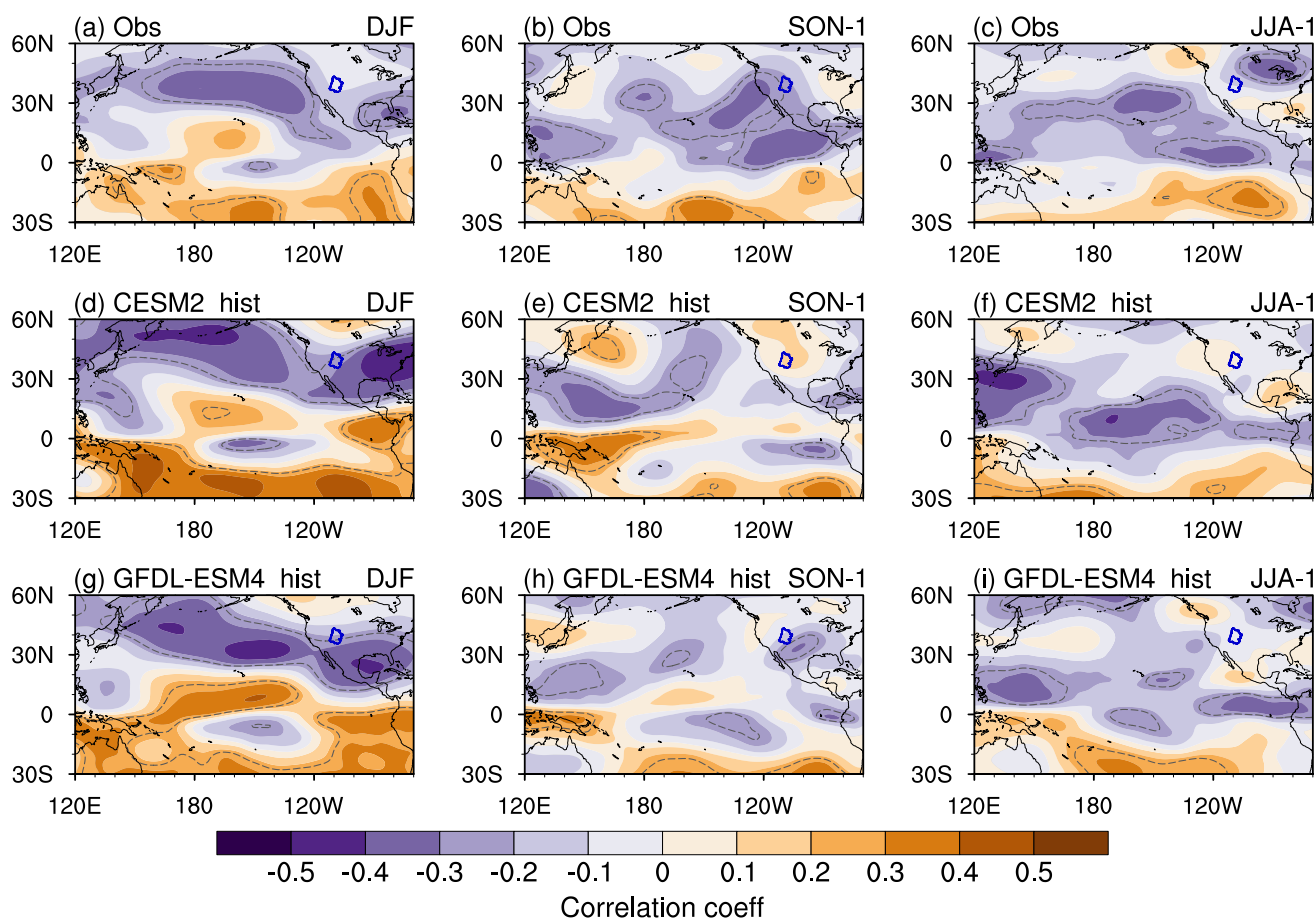
Fig. 8 Same as Fig. 4, but for correlation coefficients between UCRB domain-mean spring precipitation and previous-season streamfunction at 500 hPa

and Triacca 2011; Attanasio et al. 2013 for nonlinear and nonstationary processes).

In addition, the Granger causality approach has its own limitations (e.g., McGraw and Barnes 2018; Runge et al. 2019a). The current format of the Granger causality could only be applied to two variables, i.e., independent and dependent variables X and Y, and does not consider effects of a third or more variables. For example, the dependent variable Y is caused by another variable Z that is caused by independent variable X (X→Z→Y). In this case, Granger causality may state that X has causal effect on Y without considering the potential influence from Z. Similarly, in our study, we only detect the casual effect of SST on precipitation or precipitation on SST without including the potential influence of mediating variables such as atmospheric circulations. To understand the effect of mediating variables, one might need to apply other approaches such as Bayesian networks (Ebert-Uphoff and Deng 2012), causal effect networks (Kretschmer et al. 2016, 2020), PC momentary conditional independence (PCMCI; Runge et al. 2019a, b), temporal information partitioning networks (TIPNets; Goodwell and

Kumar 2017), etc. Another caveat of the Granger causality approach is that removing the SST term from Eq. 1 may not remove the causal effect of the lead-season SST on spring precipitation. For example, if the lead-season SST is reflected in the lead-season precipitation, then removing SST as a predictor does not necessarily remove its causal effect, which could be expressed indirectly via the lead-season precipitation term in the autoregressive model (Eq. 2).

The observational analyses in this study confirm the results of previous studies that the tropical Pacific SST from previous winter is significantly linked to the UCRB hydroclimate (e.g., Regonda et al. 2006; Switanek et al. 2009; Bracken et al. 2010; Zhao et al. 2021). As suggested in Figs. 8a and S5, the tropical winter SST and UCRB spring precipitation can be linked by atmospheric circulations. We further examine this dynamic pathway by computing the composite anomalies of SST and large-scale circulations during previous winter for anomalous years in the observation (Fig. S8). Anomalous years are those with normalized UCRB spring precipitation outside the ± 1 standard deviation. Composite anomalies are the difference between

Fig. 9 Climatological mean (mm day^{-1}) and variance ((mm day^{-1})^2) of the UCRB domain-mean spring precipitation in historical simulations and future projections of the two models
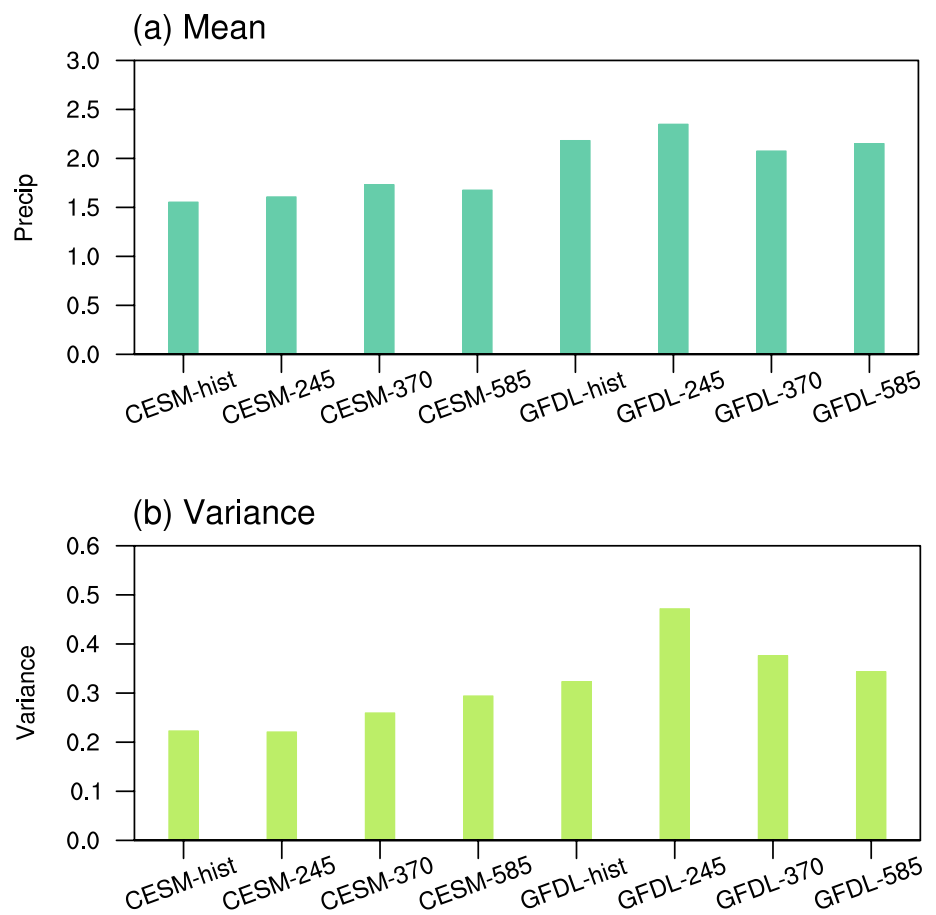

positive anomalous years and negative anomalous years. In general, the composite anomalies (Fig. S8) are consistent with the patterns of correlation (Figs. 4a and 8a), suggesting that anomalous years of the precipitation largely contribute to such correlation. Figure S8a shows a central Pacific El Niño-like SST pattern (within the Niño 3.4 region), indicating that the anomalous UCRB spring precipitation is linked to ENSO events. A persistent extended subtropic Pacific jet appears at around 30° N (Fig. S8a), accompanied by a low pressure over mid-latitude North Pacific (Fig. S8b). The low pressure favors the moisture transport from the extratropical Pacific to the western U.S. through vertically integrated horizontal water vapor flux (see the supplementary material for its calculation). Such moisture transport in previous winter can provide a wetter condition for the UCRB, leading to more precipitation in the following spring. Note that this analysis shows only evidence of the mechanism between winter SST and UCRB spring precipitation. A formal proof of the mechanism, such as prescribing the tropical SST in GCMs, is encouraged for future studies.

This study also reveals divergent projections of the causal effect of the tropical Pacific SST on the UCRB spring precipitation, especially for the high emission scenario SSP585. This finding indicates great challenges in ongoing pursuit of

reliable projections associated with ENSO variability (e.g., Stevenson 2012; Power et al. 2013; Kim et al. 2014; Chen et al. 2017). As the predictability provided by oceanic signals is still uncertain in future projections, such uncertainties may result in large uncertainties in seasonal forecasts of the UCRB hydroclimate system (e.g., precipitation and streamflow) with global climate change. Future work may consider investigating those uncertainties by analyzing more climate models.

5 Summary

This study investigates the causal effect of the tropical Pacific SST in summer, fall, and winter on the UCRB precipitation in following spring using observations and climate model simulations. The climatological mean, variability, and trend of the UCRB spring precipitation are assessed in the observation, and large values occur over mountainous regions. In historical simulations, the CESM2 and GFDL-ESM4 models well capture the spatial pattern of the climatological mean, but misrepresent the magnitude of the climatological mean and both the spatial pattern and the magnitude of variability and trend (for the period of 1950–2014). The
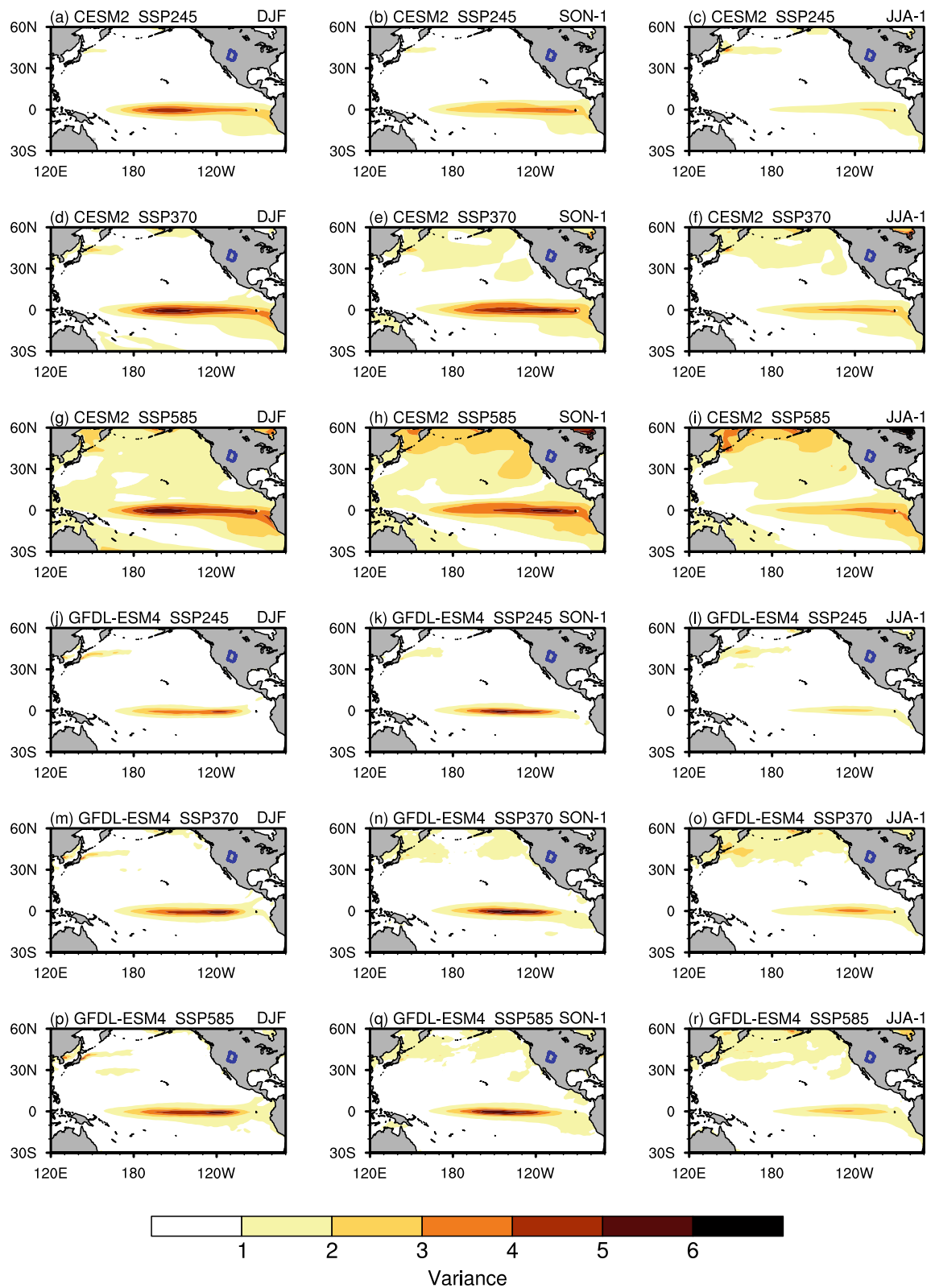
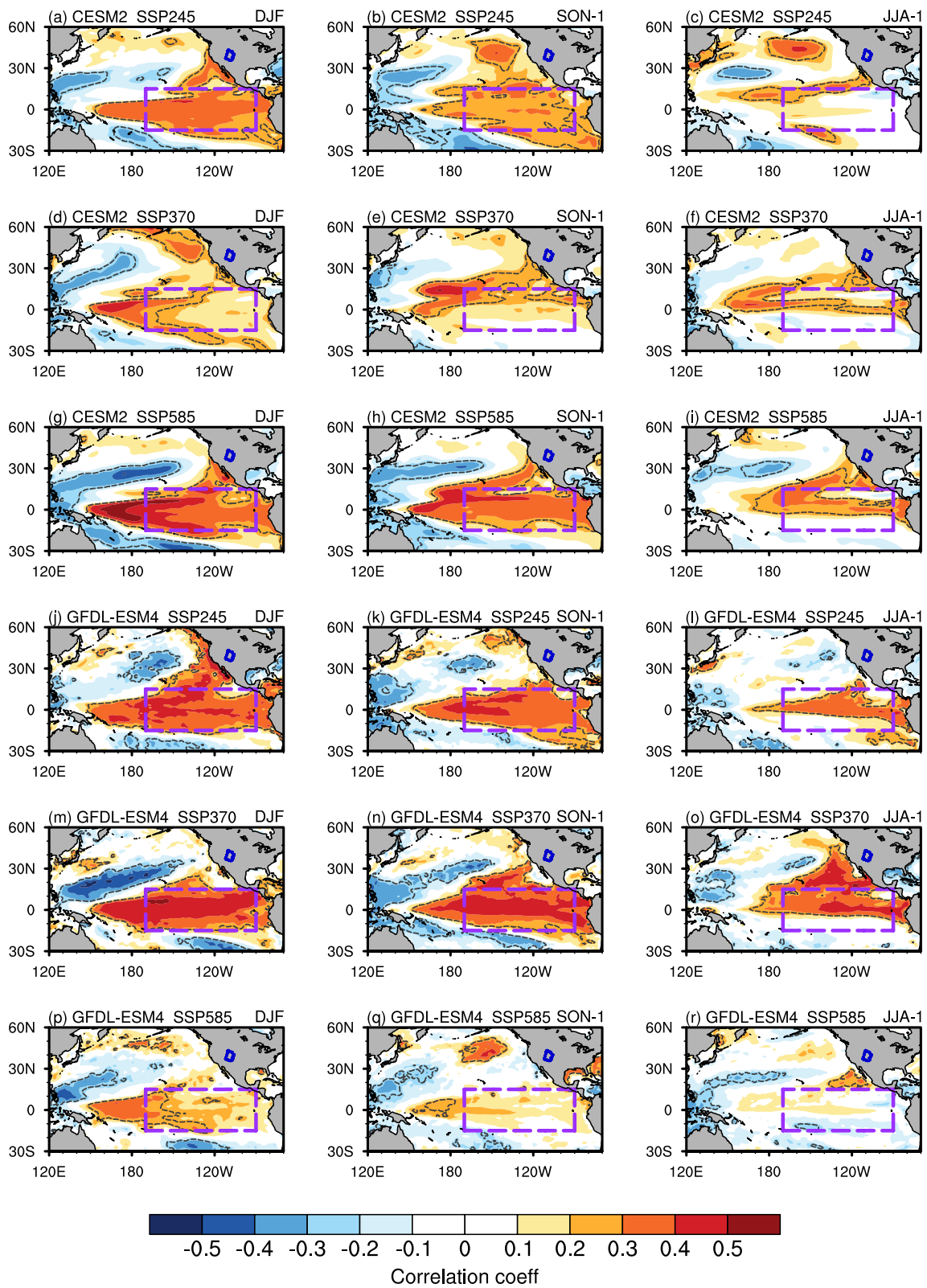**Fig. 10** Same as Fig. 3, but for future projections of the two models

Fig. 11 Same as Fig. 4, but for future projections of the two models
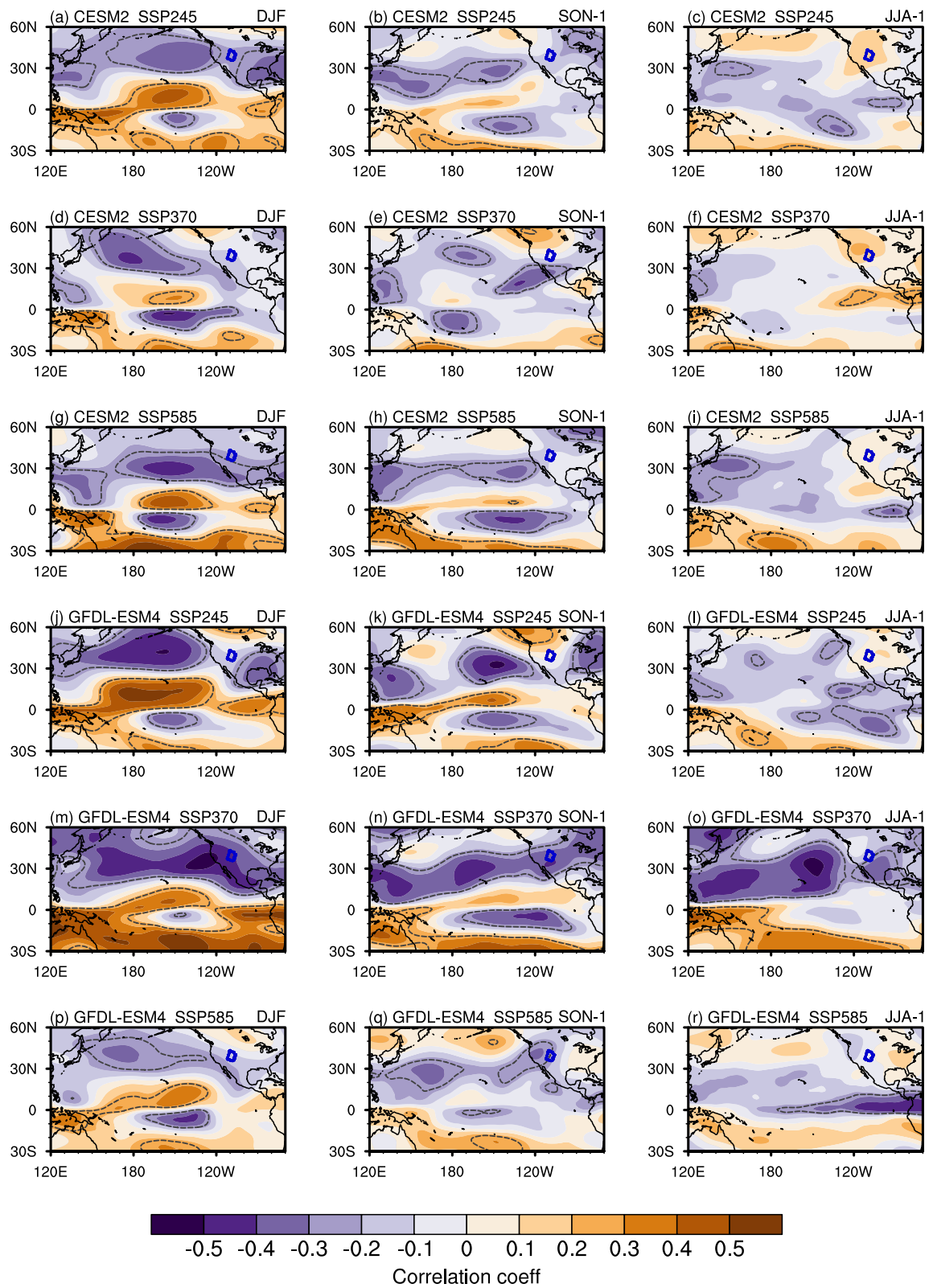
Fig. 12 Same as Fig. 8, but for future projections of the two models

SST–precipitation correlation in the observation exhibits an El Niño-like pattern for all the three lead seasons, with much lower correlation coefficients for longer lead times, while the correlation coefficients in two climate models are overestimated, especially during winter and fall.

The Granger causality approach is applied to the UCRB averaged precipitation in spring, and the UCRB averaged precipitation and the tropical Pacific averaged SST in previous three seasons. The linear trend of the time series is removed, and p-values of F-test and Chi-squared test are used to examine if the causal effect is significant. Results show that only the tropical Pacific SST in previous winter has causal effect (with p-value ~ 0.05) on the UCRB spring precipitation in the observation, while the two climate models overestimate the causal effect of previous winter (p-value < 0.01) and fall (p-value < 0.05) SST on precipitation. The comparison between historical and piControl simulations suggest that disparities between climate models and observation are likely due to model biases and external forcings in historical simulations reduce the disparities. Additional analyses show that during winter the causal effect of SST on precipitation is linked to a dipole atmospheric circulation pattern.

Finally, the Granger causality approach is applied to future projections of CESM2 and GFDL-ESM4 models and the results show divergent casual effects in the future. For the scenario with the highest anthropogenic emissions (SSP585), the p-value of the Granger causality for the CESM2 model is much smaller than that for the GFDL-ESM4 model, indicating a much stronger causal effect of SST on precipitation in the CESM2. The different causal effect in the SSP585 scenario between the two models could be attributed to two reasons. One is the different nature (e.g., variability and climatological mean) of the projected UCRB spring precipitation and tropical Pacific SST between the two models, and the other is associated with the differences in representing the precipitation–circulation connection between the two models.

Declarations

Conflict of interest None.

References

Alley R et al (2007) Summary for policymakers. Climate change 2007: the physical science basis. Cambridge University Press, Cambridge, pp 1–18

Attanasio A, Triacca U (2011) Detecting human influence on climate using neural networks based Granger causality. Theor Appl Climatol 103:103–107

Attanasio A, Pasini A, Triacca U (2013) Granger causality analyses for climatic attribution. Atmos Clim Sci 3:515–522

Ayers J, Ficklin D, Stewart I, Strunk M (2016) Comparison of CMIP3 and CMIP5 projected hydrologic conditions over the Upper Colorado River Basin. Int J Climatol 36:3807–3818

Aziz OA, Tootle GA, Gray ST, Piechota TC (2010) Identification of Pacific Ocean sea surface temperature influences of Upper Colorado River Basin snowpack. Water Resour Res 46:W07536

Barnett TP, Adam JC, Lettenmaier DP (2005) Potential impacts of a warming climate on water availability in snow-dominated regions. Nature 438:303–309

Bracken C, Rajagopalan B, Prairie J (2010) A multisite seasonal ensemble streamflow forecasting technique. Water Resour Res 46:W03532

Cai W et al (2014) Increasing frequency of extreme El Niño events due to greenhouse warming. Nat Clim Change 4:111–116

Cai W et al (2015a) ENSO and greenhouse warming. Nat Clim Change 5:849–859

Cai W, Wang G, Santoso A, McPhaden MJ, Wu L, Jin F-F, Timmermann A, Collins M, Vecchi G, Lengaigne M, England MH, Dommenget D, Takahashi K, Guilyardi E (2015b) Increased frequency of extreme La Niña events under greenhouse warming. Nature Clim Change 5:132–137

Cai W, Wang G, Dewitte B, Wu L, Santoso A, Takahashi K, Yang Y, Carréric A, McPhaden MJ (2018) Increased variability of eastern Pacific El Niño under greenhouse warming. Nature 564:201–206

Chen M, Shi W, Xie P, Silva V, Kousky V, Higgins RW, Janowiak K (2008) Assessing objective techniques for gauge-based analyses of global daily precipitation. J Geophys Res 113:D04110

Chen C, Cane MA, Wittenberg AT, Chen D (2017) ENSO in the CMIP5 simulations: life cycles, diversity, and responses to climate change. J Clim 30:775–801

Danabasoglu G et al (2020) The Community Earth System Model version 2 (CESM2). J Adv Model Earth Sys 12:e2019MS001916

Deser C, Phillips AS, Tomas RA, Okumura YM (2012) ENSO and Pacific decadal variability in the Community Climate System Model version 4. J Clim 25:2622–2651

Dunne JP et al (2020) The GFDL Earth System Model Version 4.1 (GFDL–ESM 4.1): overall coupled model description and simulation characteristics. J Adv Model Earth Sys 12:e2019MS002015

Ebert-Uphoff I, Deng Y (2012) Causal discovery for climate research using graphical models. J Clim 25:5648–5665

Ficklin DL, Stewart IT, Maurer EP (2013) Climate change impacts on streamflow and subbasin-scale hydrology in the Upper Colorado River Basin. PLoS One 8:e71297

Fleming SW, Dahlke HE (2014) Parabolic northern-hemisphere river flow teleconnections to El Niño-Southern Oscillation and the Arctic Oscillation. Environ Res Lett 9:104007

Fleming SW, Goodbody AG (2019) A machine learning metasystem for robust probabilistic nonlinear regression-based forecasting of seasonal water availability in the US west. IEEE Access 7:119943–119964

Franz K, Hartmann H, Sorooshian S, Bales R (2003) Verification of national weather service ensemble streamflow predictions for water supply forecasting in the Colorado River basin. J Hydrometeorol 4(6):1105–1118

Gautam J, Mascaro G (2018) Evaluation of Coupled Model Intercomparison Project Phase 5 historical simulations in the Colorado River basin. Int J Climatol 38:3861–3877

Goodwell AE, Kumar P (2017) Temporal Information Partitioning Networks (TIPNets): a process network approach to infer ecohydrologic shifts. Water Resour Res 53:5899–5919

Granger CWJ (1969) Investigating causal relationships by econometric models and cross-spectral methods. Econometrica 37:424–438

Harding BL, Wood AW, Prairie JR (2012) The implications of climate change scenario selection for future streamflow projection in the Upper Colorado River Basin. Hydrol Earth Syst Sci 16:3989–4007

Hidalgo HG, Dracup JA (2003) ENSO and PDO effects on hydroclimatic variations of the Upper Colorado River Basin. J Hydrometeorol 4:5–23

Hobbins M, Barsugli J (2020) Threatening the vigor of the Colorado River. Science 367:1192–1193

Hoerling M, Barsugli J, Livneh B, Eischeid J, Quan X, Badger A (2019) Causes for the century-long decline in Colorado River flow. J Clim 32:8181–8203

Hsieh W, Wu A, Shabbar A (2006) Nonlinear atmospheric teleconnections. Geophys Res Lett 33:L07714

Jacobs J (2011) The sustainability of water resources in the Colorado River basin. Bridge 41:6–12

Kalnay E et al (1996) The NCEP/NCAR 40-year reanalysis project. Bull Am Meteorol Soc 77:437–471

Kim TW, Valdés JB, Nijssen B, Roncayolo D (2006) Quantification of linkages between large-scale climatic patterns and precipitation in the Colorado River Basin. J Hydrol 321:173–186

Kim ST, Cai W, Jin FF, Santoso A, Wu L, Guilyardi E, An SI (2014) Response of El Nino sea surface temperature variability to greenhouse warming. Nat Clim Change 4:786–790

Kretschmer M, Coumou D, Donges JF, Runge J (2016) Using causal effect networks to analyze different Arctic drivers of midlatitude winter circulation. J Clim 29:4069–4081

Kretschmer M, Zappa G, Shepherd TG (2020) The role of Barents-Kara sea ice loss in projected polar vortex changes. Weather Clim Dyn 1:715–730

Lamb KW, Piechota TC, Aziz OA, Tootle GA (2011) A basis for extending long-term streamflow forecasts in the Colorado River Basin. J Hydrol Eng 16:1000–1008

McCabe GJ, Wolock DM, Pederson GT, Woodhouse CA, McAfee S (2017) Evidence that recent warming is reducing Upper Colorado River flows. Earth Interact 21(10):1–14

McGraw MC, Barnes EA (2018) Memory matters: a case for Granger causality in climate variability studies. J Clim 31:3289–3300

Meinshausen et al (2020) The shared socio-economic pathway (SSP) greenhouse gas concentrations and their extensions to 2500. Geosci Model Dev 13:3571–3605

Milly PCD, Dunne KA (2020) Colorado River flow dwindles as warming-driven loss of reflective snow energizes evaporation. Science 367:1252–1255

Mosedale TJ, Stephenson DB, Collins M, Mills TC (2006) Granger causality of coupled climate processes: ocean feedback on the North Atlantic Oscillation. J Clim 19:1182–1194

Najafi MR, Moradkhani H, Piechota TC (2012) Ensemble streamflow prediction: climate signal weighting methods vs climate forecast system reanalysis. J Hydrol 442:105–116

Newman M et al (2016) The Pacific Decadal Oscillation, revisited. J Clim 29:4399–4427

Oubeidillah AA, Tootle GA, Moser C, Piechota T, Lamb K (2011) Upper Colorado River and Great Basin streamflow and snowpack forecasting using Pacific oceanic–atmospheric variability. J Hydrol 410:169–177

Pagano TC, Garen DC, Perkins TR, Pasteris PA (2009) Daily updating of operational statistical seasonal water supply forecasts for the western U.S. J Am Water Resour Assoc 45:767–778

Power S, Delage F, Chung C, Kociuba G, Keay K (2013) Robust twenty-first-century projections of El Niño and related precipitation variability. Nature 502:541–545

Prairie J, Callejo R (2005) Natural flow and salt computation methods, calendar years 1971–1995. Bureau of Reclamation, Salt Lake City, pp 1–112

Rayner NA, Parker DE, Horton EB, Folland CK, Alexander LV, Rowell DP, Kent EC, Kaplan A (2003) Global analyses of sea surface temperature, sea ice, and night marine air temperature since the late nineteenth century. J Geophys Res 108:4407

Regonda SK, Rajagopalan B, Clark M, Zagona E (2006) A multimodel ensemble forecast approach: application to spring seasonal flows in the Gunnison River basin. Water Resour Res 42:W09404

Reynolds LV, Shafroth PB, Poff NL (2015) Modeled intermittency risk for small streams in the Upper Colorado River Basin under climate change. J Hydrol 523:768–780

Runge J et al (2019a) Inferring causation from time series in Earth system sciences. Nat Commun 10:2553

Runge J et al (2019b) Detecting and quantifying causal associations in large nonlinear time series datasets. Sci Adv 5:eaau4996

Sagarika S, Kalra A, Ahmad S (2015) Interconnections between oceanic–atmospheric indices and variability in the U.S. streamflow. J Hydrol 525:724–736

Sagarika S, Kalra A, Ahmad S (2016) Pacific Ocean SST and Z500 climate variability and western U.S. seasonal streamflow. Int J Climatol 36:1515–1533

Sheffield J et al (2013) North American climate in CMIP5 experiments. Part II: evaluation of historical simulations of intraseasonal to decadal variability. J Clim 26:9247–9290

Solander K, Bennett K, Fleming S, Gutzler D, Hopkins E, Middleton R (2018) Interactions between climate change and complex topography drive observed streamflow changes in the Colorado River Basin. J Hydrometeorol 19:1637–1650

Stevenson SL (2012) Significant changes to ENSO strength and impacts in the twenty-first century: results from CMIP5. Geophys Res Lett 39:L17703

Switanek MB, Troch PA, Castro CL (2009) Improving seasonal predictions of climate variability and water availability at the catchment scale. J Hydrometeorol 10:1521–1533

Udall B, Overpeck J (2017) The twenty-first century Colorado River hot drought and implications for the future. Water Resour Res 53:2404–2418

U.S. Bureau of Reclamation (2012) Colorado River Basin water supply and demand study, Executive summary. U.S. Department of

the Interior, https://www.usbr.gov/lc/region/programs/crbstudy/finalreport/Executive%20Summary/CRBS_Executive_Summary_FINAL.pdf. Accessed 1 Dec 2012

Vano JA, Lettenmaier DP (2014) A sensitivity-based approach to evaluating future changes in Colorado River discharge. Clim Change 122:621–634

Vano JA, Udall B, Cayan DR, Overpeck JT, Brekke LD, Das T, Hartmann HC, Hidalgo HG, Hoerling M, McCabe GJ, Morino K, Webb RS, Werner K, Lettenmaier DP (2014) Understanding uncertainties in future Colorado River streamflow. Bull Am Meteorol Soc 95:59–78

Wang H, Ting M (2000) Covariabilities of winter US precipitation and Pacific sea surface temperature. J Clim 13:3711–3719

Wang W, Anderson BT, Kaufmann RK, Myneni RB (2004) The relation between the North Atlantic oscillation and SSTs in the North Atlantic Basin. J Clim 17:4752–4759

Werner K (2011) NOAA's Colorado Basin River Forecast Center: "climate services on the Colorado River: capabilities, gaps, and chasms." Colorado River Basin Forecast Center, Salt Lake City

Werner K, Yeager K (2013) Challenges in forecasting the 2011 runoff season in the Colorado Basin. J Hydrometeorol 14:1364–1371

Woodhouse CA, Pederson GT, Morino K, McAfee SA, McCabe GJ (2016) Increasing influence of air temperature on upper Colorado River streamflow. Geophys Res Lett 43:2174–2181

Wu A, Hsieh WW, Shabbar A (2005) The nonlinear patterns of North American winter temperature and precipitation associated with ENSO. J Clim 18:1736–1752

Xiao M, Udall B, Lettenmaier D (2018) On the causes of declining Colorado Rover streamflows. Water Resour Res 54:6739–6756

Zhao S, Deng Y, Black RX (2016) Warm season dry spells in the central and eastern United States: diverging skill in climate model representation. J Clim 29:5617–5624

Zhao S, Deng Y, Black RX (2017) Observed and simulated spring and summer dryness in the United States: the impact of the Pacific sea surface temperature and beyond. J Geophys Res Atmos 122:12713–12731

Zhao S, Fu R, Zhuang Y, Wang G (2021) Long-lead seasonal prediction of streamflow over the Upper Colorado River Basin: the role of the Pacific sea surface temperature and beyond. J Clim 34:6855–6873